Three-Dimensional Homonuclear NOESY-TOCSY of an Intramolecular Pyrimidine·Purine·Pyrimidine DNA Triplex Containing a Central G·TA Triple: Nonexchangeable Proton Assignments and Structural Implications†

Ishwar Radhakrishnan and Dinshaw J. Patel*

Department of Biochemistry and Molecular Biophysics, College of Physicians and Surgeons, Columbia University, New York, New York 10032

Xiaolian Gao

Department of Structural and Biophysical Chemistry, Glaxo, Incorporated, Research Institute, 5 Moore Drive, Research Triangle Park, North Carolina 27709

Received October 10, 1991; Revised Manuscript Received December 16, 1991

ABSTRACT: Two- and three-dimensional homonuclear ^{1}H NMR spectroscopic techniques have been applied to obtain nearly complete nonexchangeable proton assignments for a 31-residue intramolecular pyrimidine·purine·pyrimidine DNA triplex containing a central G·TA triple in D_2O. An assignment strategy for obtaining resonance assignments for DNA protons from a 3D NOESY-TOCSY spectrum is proposed. The strategy utilizes the H1′/H5 ω_3 planes and relies on the recognition of cross-peak patterns for obtaining both intraresidue as well as sequential assignments. On the basis of the cross-peaks observed in the 2D and 3D spectra, a few structural features of the triplex have been delineated qualitatively. All three strands of the triplex adopt a right-handed helical conformation, and, despite the introduction of a central purine guanosine, there is no evidence for major structural distortions in the protonated third strand on the basis of a qualitative interpretation of NMR data. Several interstrand contacts between the purine and the Hoogsteen pyrimidine strands are observed which define the relative orientation of the bases and sugars in these two strands. The presence of strong NOEs between the methyl protons of thymine and the H1′ proton of guanosine defines the preferred base-pairing alignment of guanosine at the G·TA triple site. The general approaches illustrated in this study extend the range of DNA molecules accessible for detailed structural investigation by high-resolution NMR spectroscopy.

Once regarded as an in vitro artifact, triple-helical DNA has been the subject of intense study since its recognition as a potential tool for therapeutic applications and for genome mapping (Moser & Dervan, 1987; Praseuth et al., 1988; Povsic & Dervan, 1989; Maher et al., 1989; Sun et al., 1989; Luebke et al., 1989; Strobel & Dervan, 1990, 1991; Horne & Dervan, 1990; Perronault et al., 1990). Several studies have established the conditions and the energetics for triplex formation [reviewed in Wells et al. (1988), Plum et al. (1990), Xodo et al. (1990), Manzini et al. (1990), and Pilch et al. (1990)]. Novel base-pairing and triplex motifs have been identified, which has led to their classification into two different categories: the pyrimidine·purine·pyrimidine type and the more recently discovered purine·purine·pyrimidine type of triplexes (Letai et al., 1988; Griffin & Dervan, 1989; Broitman et al., 1987; Cooney et al., 1988; Kohwi & Kohwi-Shigematsu, 1988; Beal & Dervan, 1991; Chen, 1991; Pilch et al., 1991). Thus far, a high-resolution structure for triple-helical DNA belonging to either class has eluded both crystallographers and NMR spectroscopists alike. The current understanding for the pyrimidine·purine·pyrimidine class of triplexes has been restricted to a structural model proposed by Arnott and co-workers based on fiber-diffraction patterns (Arnott & Selsing, 1974; Arnott et al., 1976) and, more recently, to structural studies by NMR spectroscopy (de los Santos et al., 1989; Rajagopal & Feigon, 1989; Mooren et al., 1990; Sklenar & Feigon, 1990; Radhakrishnan et al., 1991a). These NMR approaches have recently been extended to purine·purine·pyrimidine triplexes in solution (Radhakrishnan et al., 1991b).

A detailed structural investigation using NMR techniques requires, as a first step, unambiguous assignment of almost all the resonances and cross-peaks in a spectrum (Wüthrich, 1986). The chemical shift dispersion in DNA is limited owing to the presence of only four different bases, each possessing a deoxyribose moiety, that are chemically equivalent. This results in considerable chemical shift degeneracies in molecules in excess of 30 residues, making reliable resonance and especially cross-peak assignments extremely difficult to obtain from conventional two-dimensional NMR spectroscopy. One of the solutions to this problem, first recognized and applied to proteins, has been to extend the dimensionality by incorporating an additional magnetization transfer process involving either the same or a different nucleus (Greisinger et al., 1987a; Oschkinat et al., 1988; Fesik & Zuiderweg, 1988). Since then, a range of three-dimensional experiments have been proposed and applied successfully to a variety of biological systems (Greisinger et al., 1987b, 1989; Oschkinat et al., 1989a,b; Vuister et al., 1988; Boelens et al., 1989; Breg et al., 1990; Padilla et al., 1990; Zuiderweg & Fesik, 1989; Marion et al., 1989). Among the homonuclear experiments, the NOESY-TOCSY and the TOCSY-NOESY experiments have found favor among spectroscopists as they combine, in a single experiment, two distinct processes that are regularly used to obtain both spectral assignments as well as structural information.

A typical 3D homonuclear experiment produces a multitude of cross-peaks in the 3D spectrum rendering it very complex

† This research was supported by NIH Grant GM34504 to D.P.

* To whom correspondence should be addressed.

0006-2960/92/0431-2514$03.00/0

for analysis without the use of an effective assignment strategy. For proteins, a host of strategies for assigning proton resonances and for resolving superimposed cross-peaks have been proposed for different 3D experiments (Breg et al., 1990; Padilla et al., 1990; Vuister et al., 1990; Gao & Burkhart, 1991). To date, three reports where 3D homonuclear experiments have been performed on DNA oligomers have appeared in the literature (Boelens et al., 1989; Piotto & Gorenstein, 1991; Mooren et al., 1991), and only the most recent report addresses the problem of securing assignments for DNA protons from the ω_2 planes corresponding to the H2″ resonances by recognizing spin-lock coupling patterns in a 3D TOCSY-NOESY spectrum (Mooren et al., 1991).

Pursuant to our earlier characterization of an intramolecular pyrimidine·purine·pyrimidine triplex (designated the G·TA triplex; Chart I) in H_2O (Radhakrishnan et al., 1991a), we have extended our studies on the same triplex in D_2O under similar conditions using 2D and 3D NMR spectroscopic methods as a part of our efforts to determine the complete three-dimensional structure of the molecule. In this paper, we shall discuss in detail a general and practical procedure for assigning DNA protons in a 3D NOESY-TOCSY spectrum that leads to an almost complete assignment of DNA protons in the 31-residue oligomer. Also, a few structural features of the triplex under study will be highlighted.

Materials and Methods

Oligonucleotide Synthesis. The 31-mer deoxyoligonucleotide was synthesized on a 10-μmol scale on an Applied Biosystems 391 DNA Synthesizer using the β-cyanoethylphosphoramidite chemistry. The isolation and purification procedures have been described previously (de los Santos et al., 1989). The NMR studies were conducted on approximately 4 mM concentration of the oligomer in the presence of 0.1 mM EDTA and 10 mM phosphate buffer adjusted to pH 4.9.

NMR Experiments. All the NMR experiments on the G·TA triplex in D_2O at 25 °C were performed either on a Bruker AMX500 spectrometer at Glaxo or on a Bruker AM500 spectrometer at Columbia University. The mixing periods for the NOESY and TOCSY sequences in the 3D NOESY-TOCSY experiment (Vuister et al., 1988) were 200 and 28 ms, respectively. A sweep width of 4201.7 Hz (8.4 ppm) was used in all three dimensions. The data were acquired with 256 × 66 × 128 complex points in the t_3, t_2, and t_1 time domains, respectively. Sixteen scans were recorded for each FID. Data processing was carried out as described previously (Gao & Burkhart, 1991), and the resulting size of the matrix was 256 × 256 × 256 in real points.

All 2D experiments were recorded under identical ambient conditions using similar experimental parameters as in the 3D experiment. Quadrature was simulated in the t_1 domain using either the States or TPPI modes. A total of 256 complex data points were collected along the t_1 dimension for the NOESY spectra recorded with mixing times of 50 and 250 ms. DQF-COSY, COSY-36, and ω_1-scaled COSY-45 spectra with 256, 476, and 460 complex t_1 points were also acquired. The data were processed with FTNMR and FELIX software packages (Hare Research, Inc.) on a VAX 6310 computer and a Silicon Graphics 4D/35 workstation, respectively. All chemical shifts were referenced relative to the chemical shift of the residual solvent signal (4.76 ppm) at 25 °C.

Results

The sequence and the numbering scheme for the pyrimidine·purine·pyrimidine intramolecular triplex containing a central G·TA triple is shown in Chart I. The molecule consists of 31 nucleotides with a stem region made up of seven base triples and two loops of five residues each. The complete one-dimensional spectrum of the G·TA triplex in D_2O at 25 °C is shown in Figure 1A. An expanded plot of the base and H1′/H5 proton region of the same spectrum is shown in Figure

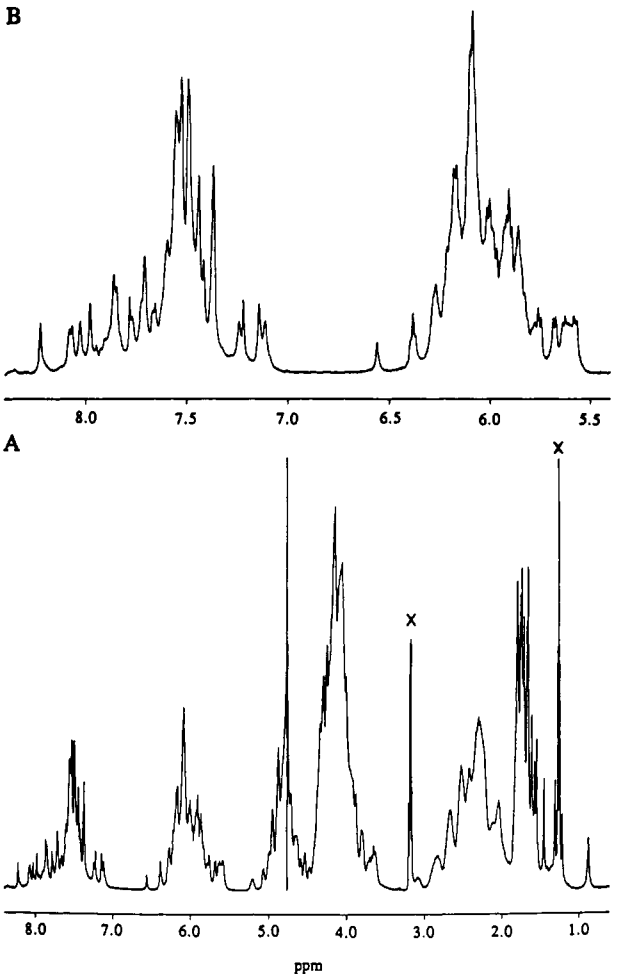

FIGURE 1: (A) Complete one-dimensional ^{1}H NMR spectrum of the G·TA triplex recorded in D_2O at 25 °C, pH 4.9, in 0.1 mM EDTA, 10 mM PO_4 buffer. Extra peaks from the residual triethylammonium buffer used during the purification process have been denoted by an X. (B) An expanded plot of the aromatic and the H1′ proton region of the same spectrum.

Chart I

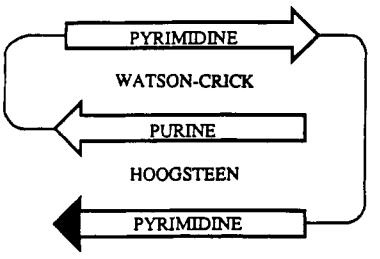

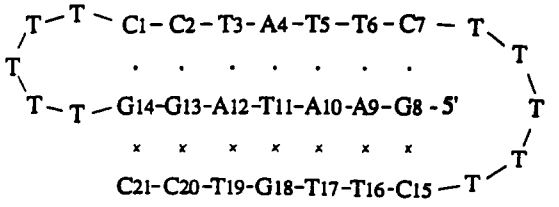

1B. Notice the enhanced spectral resolution and dispersion in these regions over the other regions of the spectrum.

3D Spectral Characteristics. The distinctive features of a 3D spectrum have been documented extensively (Greisinger et al., 1987a, 1989; Vuister et al., 1988, 1990; Oschkinat et al., 1989a; Breg et al., 1990), and we shall, by means of a brief introduction, focus only on related aspects dealing with the origin and interpretation of cross-peaks in a 3D spectrum. The "true" 3D cross-peaks are those seen at positions ($\omega_1 \neq \omega_2 \neq \omega_3$) which result from two steps of magnetization transfer. These cross-peaks label the nuclei that participated in the transfer process. Thus the three frequency coordinates (ω_1, ω_2, ω_3) of a 3D cross-peak represent the source (ω_1), the intermediate (ω_2), and the destination (ω_3) nuclei, respectively. In the 3D NOESY-TOCSY experiment, the first step is an incoherent transfer driven by dipolar coupling, while the second involves a coherent transfer between scalar coupled spin pairs. The intensity of the cross-peak is modulated by the efficiency of these consecutive transfer processes. Cross-peaks are also encountered in the three cross-diagonal planes: the NOESY, TOCSY, and back-transfer planes in the 3D spectrum. To conduct an analysis, 2D cross-sections are taken perpendicular to any of the three orthogonal frequency axes of the 3D spectrum. Most of our discussion will be confined to planes taken perpendicular to the ω_3 axis since the highest digital resolution is afforded by this dimension and the residual water signal is better suppressed.

The cross-peaks in the ω_3 plane establish the correlation that a spin ($\delta = \omega_3$) is scalar coupled to a spin ($\delta = \omega_2$) which in turn is dipolar coupled to another spin ($\delta = \omega_1$). Therefore, all the "true" 3D cross-peaks which appear in the ω_3 plane of a given proton Hx in a 3D NOESY-TOCSY spectrum can be interpreted as NOEs involving protons coupled through-bond with the proton Hx. The intensities of the cross-peaks are modulated by the through-bond coupling. Conversely, the "true" 3D cross-peaks in the ω_1 plane of the Hx proton can be regarded as TOCSY cross-peaks shown by protons coupled through-space with proton Hx.

3D NOESY-TOCSY Spectral Features of DNA. The ω_3 planes corresponding to the H8/H6 base proton resonances in the 3D spectrum yield little or no new information relative to their 2D counterparts. This is due to the absence of an efficient two-step transfer involving these protons which precludes the observation of "true" 3D cross-peaks. In other words, only "pure" NOE cross-peaks between these base and other protons are observed except for cytidine H6 planes where through-space correlations of the H5 proton with other protons can also be observed. The former set of cross-peaks are seen on the NOE line, while the latter appear on a line (ω_2 = H5) parallel to the NOE line.

A completely different situation prevails in the H1′ ω_3 planes. Numerous off-diagonal cross-peaks can be observed with reasonable intensity, especially in the H2′,2″ region along the ω_2 axis (see below). This is not surprising because in canonical B-DNA the H1′ proton exhibits strong scalar coupling with the H2′,2″ protons, ca. 6–10 Hz (Wüthrich, 1986). Also the H2′,2″ protons are spatially situated in a favorable position to participate in dipolar interactions with not only several intraresidue protons but with interresidue base protons as well. These considerations along with the fact that H1′ resonances are the most well resolved compared to all the other sugar protons led to the selection of the H1′ planes for obtaining resonance assignments.

The cytidine H5 planes, which are also located in the H1′ ω_3 region, display cross-peaks which permit through-space

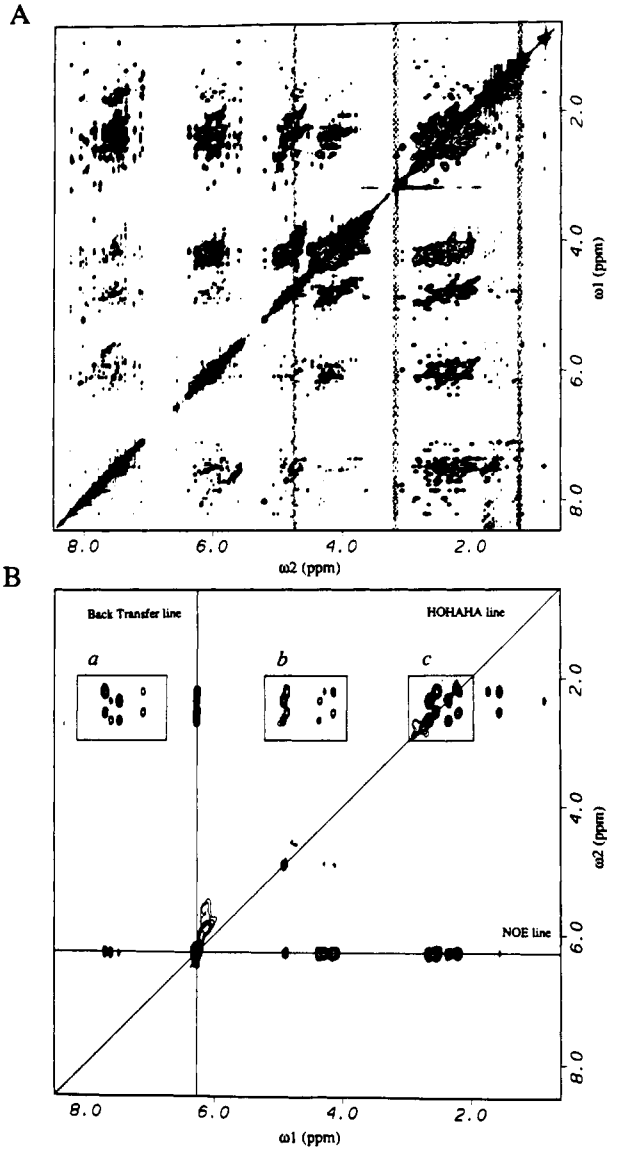

FIGURE 2: (A) Survey plot of the 2D NOESY (τ_m = 250 ms) spectrum of the G·TA triplex recorded in D_2O at 25 °C, pH 4.9, in 0.1 mM EDTA, 10 mM PO_4 buffer. (B) An ω_3 plane corresponding to the superpositioned H1′ resonances of T16 and T19 (ω_3 = 6.27 ppm) taken from the 3D NOESY-TOCSY (NOESY τ_m = 200 ms) spectrum of the G·TA triplex recorded under similar conditions. The three lines which result from intersection with the cross-diagonal planes are shown. Boxed regions correspond to base–H2′,2″ (a), H3′,H4′,H5′,5″–H2′,2″ (b), and the symmetrical H2′,2″ region (c).

correlations to be made exclusively for cytidine H6 protons—a feature recognized by an earlier study (Piotto & Gorenstein, 1991). These cross-peaks involving H5 protons appear in the lower diagonal of the ω_3 plane in contrast to the NOE correlations through H2′,2″ protons seen in the upper diagonal of the H1′ planes.

The spectral simplification achieved in a 3D NOESY-TOCSY spectrum of the G·TA triplex is shown in Figure 2B, where a survey plot of a representative H1′ ω_3 plane taken from the 3D spectrum is compared with the 2D NOESY spectrum (Figure 2A) recorded under similar ambient conditions. Notice the considerable reduction in overlap in the base–H2′,2″ region of the H1′ plane (box a, Figure 2B). Also notice the enhanced clarity in the H3′,H4′,H5′,5″–H2′,2″ regions of the H1′ plane over the 2D spectrum (box b, Figure 2B). The pathways through which these cross-peaks arise are schematically shown in Figure 3. Following the notation introduced by Vuister et al. (1990), cross-peaks in the 3D spectrum

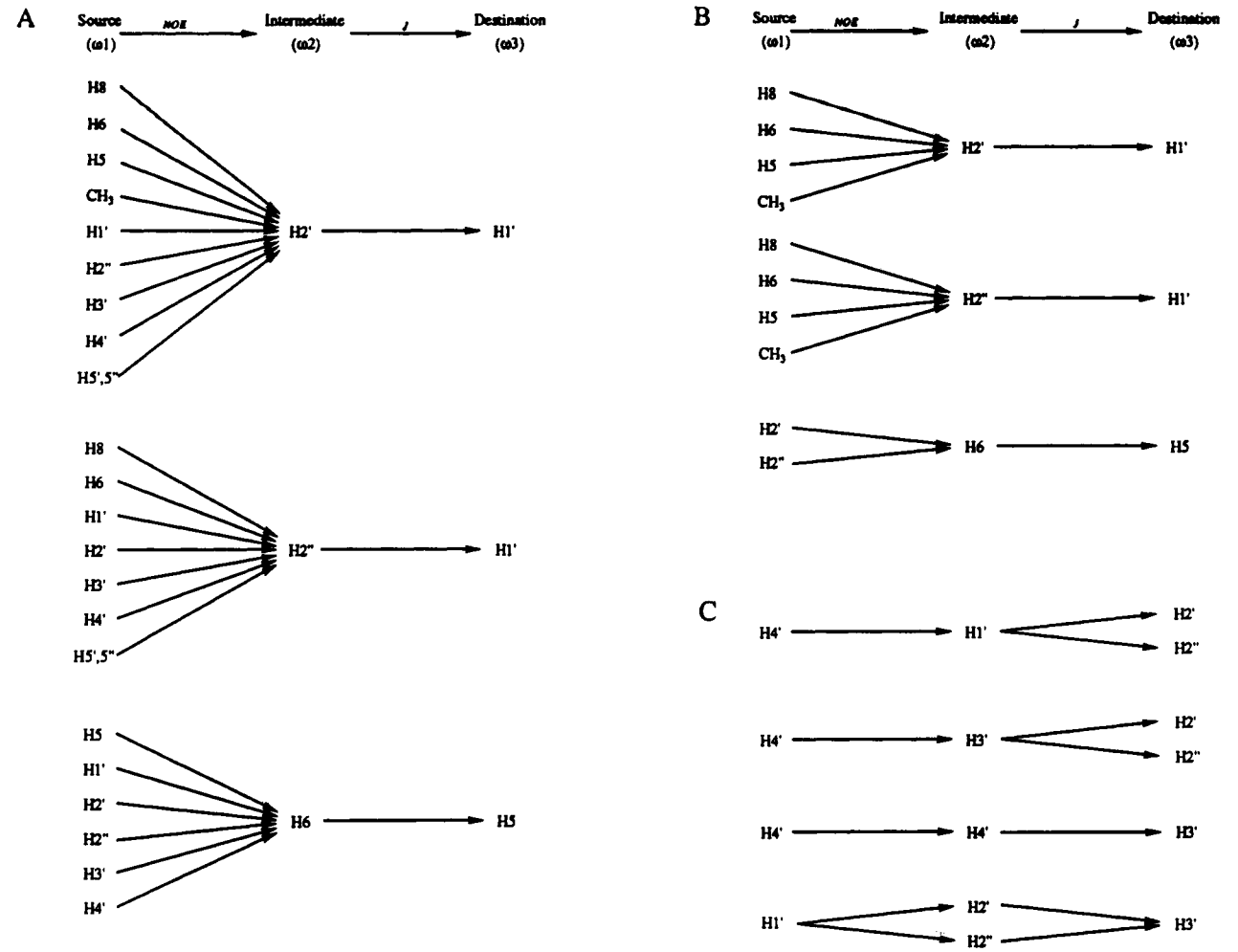

FIGURE 3: Relevant magnetization transfer pathways for obtaining assignments for DNA protons in a 3D NOESY-TOCSY spectrum. The resulting cross-peaks can be seen in the 2D cross-sections corresponding to any of the three frequency coordinates of the cross-peak. (a) Intraresidue transfers mediated by the H2′,2″ and H6 protons to the H1′ and H5 protons. (b) Pathways important for tracing sequential connectivities in the H1′/H5 planes. (c) Some intraresidue transfer pathways useful for confirming the assignments made for the H3′ and H4′ protons.

will be labeled $C_{abc}(i,j,k)$ where the subscripts a, b, and c refer to the nucleus in residues i, j, and k, respectively. In this notation, spins a_i and b_j are related through-space while spins b_j and c_k are coupled through-bond.

Sequential Assignment Protocol. The conventional resonance assignment process in DNA relies on tracing sequential connectivities in the base–H1′ fingerprint region of a 2D NOESY spectrum. Instead, our procedure for making sequential assignments in a 3D NOESY-TOCSY spectrum is based on tracing the sequential NOE connectivities in the base–H2′,2″ region of the H1′ ω_3 planes (Radhakrishnan et al., 1991c). In these planes, distinct spectral patterns involving H2′,2″ proton pairs can be recognized. Each H2′,2″ pair shows strong geminal cross-peaks in the symmetrical H2′,2″ region of the 2D plane (box c, Figures 2B and 4), as well as strong and moderate cross-peaks with both intra- and interresidue base and other intraresidue sugar protons, respectively (boxes a and b, Figures 2B and 4). These characteristic cross-peak patterns permit the identification of the number of H2′,2″ pairs which correlates with the number of H1′ protons in each H1′ ω_3 plane. This is critical for analysis due to interference from the so-called "cross-talk" cross-peaks (see below). Additionally, thymine residues can be identified by the presence of CH_3–H2′ NOE cross-peaks in the H1′ ω_3 planes. Likewise, cytidine residues can be distinguished by analyzing their characteristic H5 planes. For the purposes of bookkeeping and cross-peak assignment, it is helpful to maintain a database where the location of all the cross-peaks in each of the H1′ planes are documented.

For making sequential assignments, the base–H2′,2″ region in the H1′ ω_3 planes are used in conjunction with the H1′–H2′,2″ region in the base proton ω_1 planes. It needs to be emphasized that both of these regions span the same subspace in the 3D spectrum, only they are viewed differently. The logic of the sequential assignment protocol is outlined in Figure 5. Starting at the H1′ plane of residue i, the sequential base proton of residue i+1 (the order of the residues i and i+1 are arbitrarily assigned at this point) can be identified by the presence of interresidue cross-peaks between the H2′,2″ protons of residue i and the base proton of residue i+1. In the next step, the ω_1 plane corresponding to the base proton resonance of residue i+1 is inspected. In the H1′–H2′,2″ region of this plane, connectivities $C_{H8,H2'/2'',H1'}(i+1,i,i)$ and $C_{H8,H2'/2'',H1'}(i+1,i+1,i+1)$ can be found. This leads to the assignment of the H1′ and the H2′,2″ protons belonging to residue i+1. The same procedure is repeated until the tracing of sequential connectivities is no longer possible. Since specific assignments for residues i and i+1 are not made, the tracing could proceed either from the 5′ to the 3′ end or vice versa.

Sequence-specific assignments can be made if the terminal residues can be identified. The 3′ terminus can be distinguished by the presence of only one instead of two pairs of cross-peaks in the base–H2′,2″ region of its H1′ plane, provided either the H1′ or the H2′,2″ protons are resolved. On the other

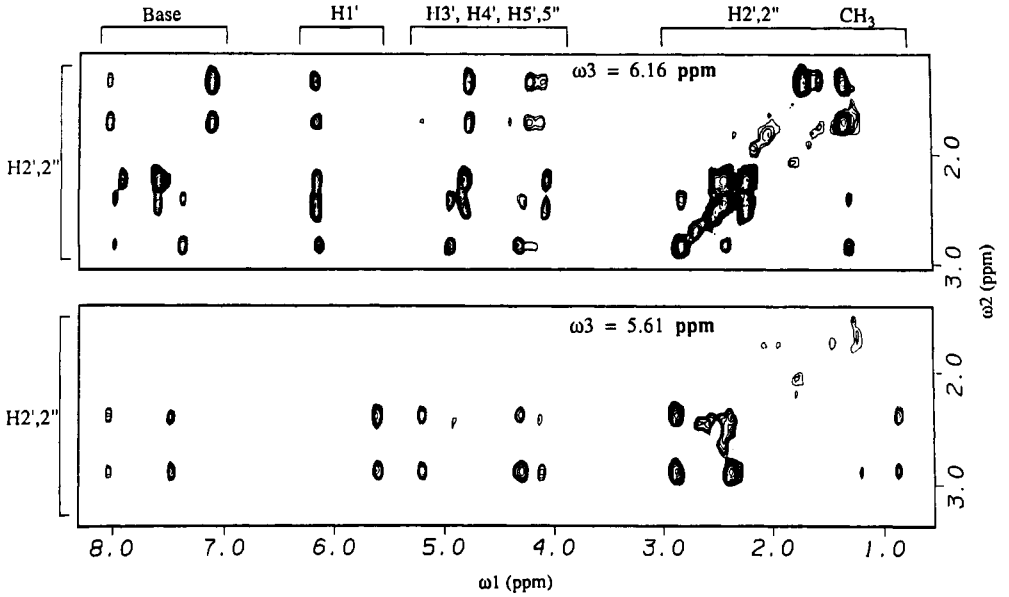

FIGURE 4: Expanded contour plots of the H1′ ω_3 planes of residues T17 (top) and G18 (bottom) in the 3D NOESY-TOCSY spectrum of the G·TA triplex. The cross-peak patterns in these regions are typical of the H1′ ω_3 planes.

hand, the 5′ end of a helical segment can identified by the presence of a single pair of cross-peaks in the H1′–H2′,2″ region in the base proton ω_1 plane. Additionally, information regarding the position of thymine and cytidine residues (see above) obtained from the process of sequential assignments, when taken in conjunction with the sequence information, can aid in sequence-specific assignments.

Sugar Proton Assignments. Once all the H1′ and H2′,2″ resonances have been assigned, resonance assignments for the intraresidue H3′ and H4′ protons can be obtained in the same H1′ planes on the basis of connectivities of the type $C_{x,H2'/2'',H1'}(i,j,j)$, where x could be either H3′ or H4′ protons (Figure 4). Initially, the H4′ proton is tentatively assigned to the same residue as the H2′,2″ protons. The assignments for the H4′ protons can then be confirmed by the presence of the $C_{H4',H1',H2'/2''}(i,i,i)$ and $C_{H4',H3',H2'/2''}(i,i,i)$ connectivities in the ω_1 or ω_3 planes (Figure 3C). Similarly, the assignments for H3′ and H4′ protons can be placed on more solid ground by also looking at the ω_1 and ω_3 planes for $C_{H3',H4',H4'}(i,i,i)$ and $C_{H1',H2'/2'',H3'}(i,i,i)$ connectivities (Figure 3C). Assignments for the H5′,5″ protons could proceed from the H4′ ω_3 plane through $C_{H5'/5'',H5''/5',H4'}(i,i,i)$ connectivities. However, in practice, the extensive overlaps in the H4′, H5′,5″ region for large systems and the chemical shift degeneracy of the H5′,5″ protons often prevent unambiguous assignments even in a 3D data set.

Proton Assignments for the DNA Triplex. As an illustration of the assignment strategy (Figure 5), we have traced out the sequential connectivities in the 3D spectrum for the segment extending from C15 to G18 in the third strand of the intramolecular triplex (Figure 6, left panel). Starting at the H1′ plane of C15, we can identify the cross-peaks $C_{H6,H2',H1'}(15,15,15)$ and $C_{H6,H2'',H1'}(15,15,15)$ on the basis of the assignment for the H6 proton made beforehand from 2D NOESY spectra in H_2O. The same pair of H2′,2″ protons show NOEs to another base proton in the same region which corresponds with the H6 resonance of T16. The H1′ resonance of T16 is located by inspecting the ω_1 plane of T16 H6 proton (Figure 5). This part of the procedure is not shown in Figure 6 for clarity. In the base–H2′,2″ region of the H1′ plane of T16, connectivities $C_{H6,H2',H1'}(16,16,16)$, $C_{H6,H2',H1'}(17,16,16)$, $C_{H6,H2'',H1'}(16,16,16)$, and $C_{H6,H2'',H1'}(17,16,16)$ could be ob-

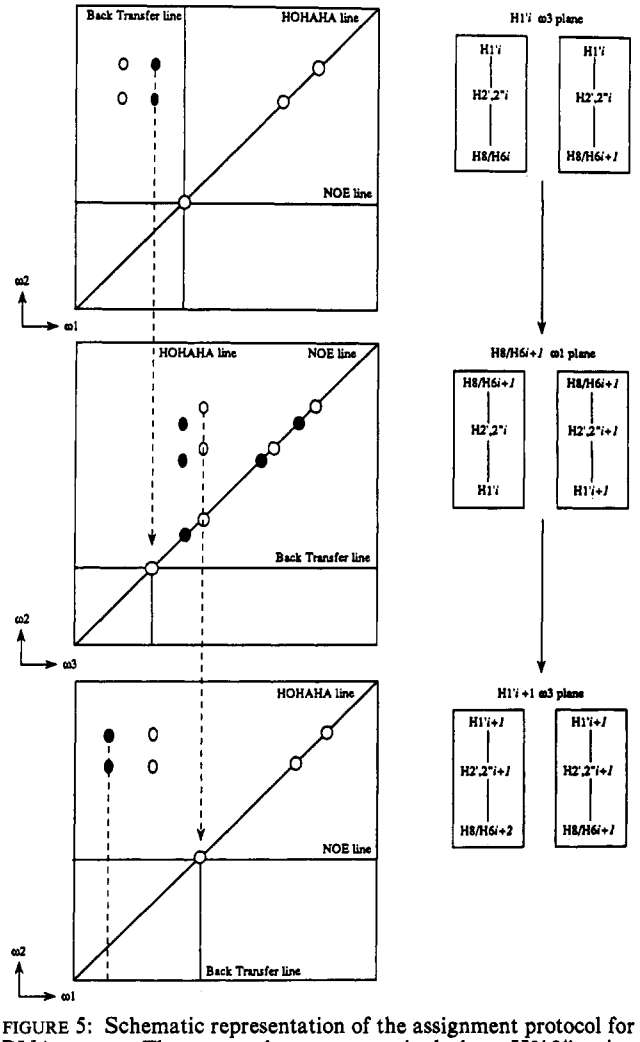

FIGURE 5: Schematic representation of the assignment protocol for DNA protons. The cross-peak patterns seen in the base–H2′,2″ region of the H1′ ω_3 planes and the H1′–H2′,2″ region of the base ω_1 planes are shown in the left panel. All cross-peaks arising from intraresidue transfers are shown with open circles, while filled circles denote sequential cross-peaks. The 3D correlations for each pair of cross-peaks are given in the right panel. These correlations are used to identify the sequential base H8/H6, H1′, and H2′,2″ protons as discussed in the text.

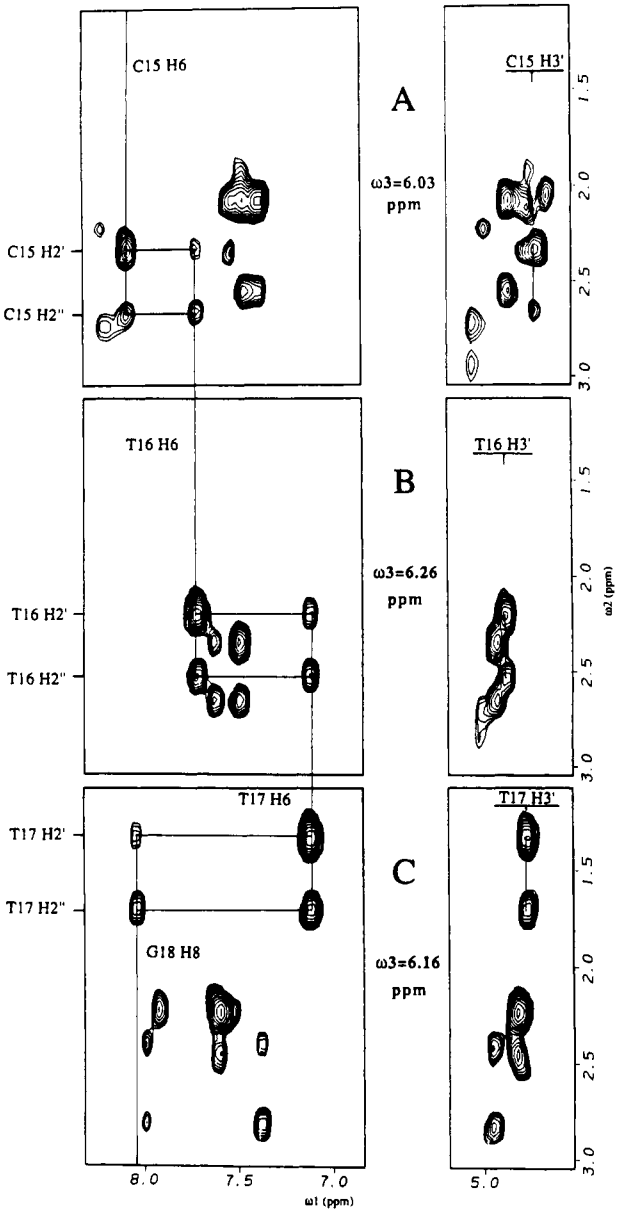

FIGURE 6: Sequential tracing of connectivities using the assignment procedure for DNA protons illustrated for the G·TA triplex. Expanded contour plots of the base–H2′,2″ (left panel) and H3′–H2′,2″ regions (right panel) viewed in the H1′ ω_3 planes of residues C15 (A), T16 (B), and T17 (C) in the 3D NOESY-TOCSY spectrum. The intermediate steps, which involves ω_1 planes of base protons (Figure 5), are not shown for clarity.

served, which identifies the H6 resonance of T17. Moving to the H1′ plane of T17, we once again see both intraresidue and sequential cross-peaks between the base and H2′,2″ protons, which leads to the assignment for the H8 proton of G18.

The assignment process outlined above was not used to make de novo assignments but rather used for the purpose of experimentation, to trace sequential connectivities and confirm the assignments made for some of the base, H1′, and H2′,2″ protons from the 2D data sets. In these 2D data sets, not all these protons were identified unambiguously, and the cross-peaks involving the remaining protons were obscured by overlaps. Using the 3D assignment procedure, on the other hand, allowed unambiguous identification of all these proton types in the 3D data set. More significantly, the 3D data set permitted assignments for the H3′ and H4′ protons of almost all the 31 residues in the sequence (Table I). This is accomplished for the H3′ protons, for example, as shown in Figure 6 (right panel).

Table I: ^{1}H Chemical Shifts for Nonexchangeable Protons in the G·TA Triplex at 25 °C in D_2O, pH 4.9

residue	H8/H6	H2	H5/CH_3	H1′	H2′, H2″	H3′	H4′
C1	7.72		5.75	5.90	2.34, 2.52	4.83	4.23
C2	7.66		5.67	6.09	2.33, 2.71	4.73	4.24
T3	7.57		1.79	6.08	2.41, 2.88	4.93	4.24
A4	7.97	7.21		6.15	2.44, 2.84	4.94	4.33
T5	7.37		1.32	6.05	2.09, 2.57	4.84	4.20
T6	7.44		1.62	6.07	2.12, 2.55	4.53	4.13
C7	7.54		5.57	6.08	2.10, 2.31	4.82	4.23
G8	7.86			5.99	2.55, 3.09	4.86	4.28
A9	7.77	7.52		6.09	2.68, 3.17	5.05	4.30
A10	8.21	7.79		6.08	2.23, 2.71	4.99	4.30
T11	7.23		1.22	5.92	2.24, 2.67	4.94	4.17
A12	7.47	6.57		5.87	2.23, 2.81	4.71	4.46
G13	7.41			5.78	2.50, 2.67	4.88	4.33
G14	7.49			5.93	2.41, 2.63	4.78	4.10
C15	8.07		6.18	6.02	2.36, 2.68	4.72	4.32
T16	7.70		1.75	6.26	2.22, 2.55	4.87	4.29
T17	7.11		1.58	6.18	1.36, 1.71	4.77	4.21
G18	8.02			5.61	2.40, 2.90	5.19	4.28
T19	7.48		0.88	6.28	2.37, 2.67	4.92	4.36
C20	7.61		5.62	5.92	2.14, 2.63	4.71	4.34
C21	7.85		5.90	6.38	2.24, 2.35	4.51	4.13
TL1	7.14		1.45	5.90	2.00, 2.35	4.73	4.09
TL2	7.56		1.80	6.21	2.28, 2.49	4.76	
TL3	7.55		1.76	6.12	2.04, 2.32	4.73	4.18
TL4	7.54		1.81	5.83	1.95, 2.27	4.59	
TL5	7.53		1.74	6.02	2.08, 2.35	4.78	4.16
TL1′	7.49		1.71	5.99	2.03, 2.32	4.64	4.14
TL2′	7.49		1.66	5.96	2.04, 2.27	4.64	
TL3′	7.43		1.68	6.09	2.27, 2.42	4.75	
TL4′	7.37		1.66	5.82	1.90, 2.23	4.58	
TL5′	7.36		1.55	5.85	2.03, 2.37	4.71	

Table II

pyrimidine strand (residues 15–21)	purine strand (residues 8–14)	2D NOESY	3D NOESY-TOCSY
Cross-Strand NOEs Involving Protons in the Third Strand of the G·TA Triplex[a]			
T16 NH3	G8 H2′,2″	m	*b*
T17 NH3	A9 H2′,2″	m	*b*
T19 NH3	T11 H2′,2″	m	*b*
T16 NH3	A9 H2′	w	*b*
T17 NH3	A10 H2′	w	*b*
T19 NH3	A12 H2′	ov	*b*
T16 H1′	G8 H8	w	*c*
T17 H1′	A9 H8	w	w
G18 H1′	A10 H8	ov	w
C20 H1′	A12 H8	w	w
C21 H1′	G13 H8	w	*c*
G18 H1′	T11 CH_3	s	s
G18 H2′,2″	T11 CH_3	w	w
Interresidue Sugar Proton NOEs Observed in the Third Strand of the G·TA Triplex			
T17 H2″	G18 H3′	w	w
T17 H2″	G18 H5′/5″	ov	w

[a] NOEs involving exchangeable protons are from a 2D NOESY spectrum (τ_m = 170 ms) recorded in H_2O. NOEs between nonexchangeable protons are from a 2D NOESY spectrum (τ_m = 250 ms) and a 3D NOESY-TOCSY spectrum (τ_m = 200 ms). Cross-peaks are classified as s, strong; m, moderate; w, weak; ov, overlapped. [b] NOEs involving exchangeable protons, thus not observable in spectra recorded in D_2O. [c] Cross-peaks not detected.

Unusual NOEs Observed in the G·TA Triplex. Several unusual NOEs are observed which have been assigned to protons belonging to the third strand of the triplex as shown in Table II. Some of the NOEs involving imino and sugar protons in Table II were identified previously in the 2D NOESY spectra recorded in H_2O but remained unassigned at that time (Radhakrishnan et al., 1991a). The thymidine

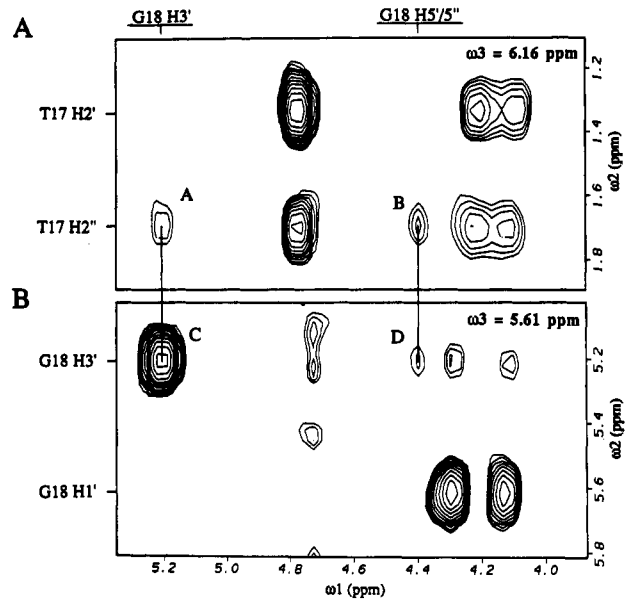

FIGURE 7: Unusual interresidue NOEs seen between the sugar protons of residues T17 and G18 in the G·TA triplex. (A) Expanded contour plot of the H2′,2″–H3′,H4′,H5′,5″ region of the H1′ ω_3 plane of residue T17 in the 3D NOESY-TOCSY spectrum: A, T17 H2″–G18 H3′; B, T17 H2″–G18 H5′/5″. (B) Expanded contour plot of the H1′,H3′–H3′,H4′,H5′,5″ region of the H1′ ω_3 plane of residue G18 in the same spectrum: C, diagonal peak of G18 H3′; D, G18 H3′–G18 H5′/5″.

imino protons of T16, T17, and T19 in the third strand show NOEs of medium intensity to the H2′,2″ protons of G8, A9, and T11 as well as weak NOEs to the H2′ protons of residues A9, A10, and A12, respectively. The other unusual NOEs involve nonexchangeable protons. One set of weak NOEs have been assigned to the base H8 protons of residues G8, A9, A10, A12, and G13 in the purine-rich strand and the H1′ sugar protons of residues T16, T17, G18, C20, and C21, respectively, in the protonated pyrimidine strand of the triplex (Table II). At the site of the G·TA triple, a strong NOE is detected between the CH_3 protons of T11 and the H1′ proton of G18 (observable even in a 50-ms 2D NOESY spectrum). Weak NOEs are also observed between the T11 methyl protons and the sugar H2′,2″ protons of G18. Unusual interresidue NOEs between sugar protons are also observed between the H2″ proton of T17 and the H3′ and H5′/5″ protons of G18 (Table II, Figure 7).

DISCUSSION

Application of Homonuclear 3D NMR Techniques to Structural Studies of DNA Molecules. Our studies on a 31-residue oligonucleotide fragment demonstrate the utility of a homonuclear 3D NOESY-TOCSY ^1H NMR spectrum for making unambiguous resonance and cross-peak assignments pertinent to the structural information of DNA. This is the first example where nearly complete proton assignments (Table I) have been obtained from a 3D homonuclear NMR data analysis for an oligodeoxyribonucleotide fragment of this size and complexity. The simplification of data achieved most notably in the H1′ ω_3 planes underscores the usefulness of a 3D proton–proton correlation spectrum. Our protocol emphasizes the use of these planes for resonance assignments of right-handed DNA through cross-peak pattern recognition and sequential connectivities, and the basic principles can be extended to the interpretation of similar homonuclear 3D experiments of nucleic acid molecules. An analysis of just these H1′ planes, as we have shown, can yield assignments for a majority of DNA protons quickly and almost always unambiguously. The assignments obtained for H3′, H4′, and some of H5′,5″ sugar protons represents a major advance over 2D NMR technology, since extensive overlaps in the spectral region of these protons in a 2D data set of moderately sized DNA molecules prevents their definitive assignments. Furthermore, since both H2′,2″ sequential connectivities are traced, even if one of them is overlapped, the resolution of the other proton in the same region allows the assignment process to continue.

A homonuclear 3D spectrum is replete with redundant information. The various regions of the spectrum is helpful for cross-checking assignments, resolving overlaps, and obtaining additional assignments and structural information. With the development of assignment strategies like the one we proposed for DNA protons which make use of recognizing distinct spectral patterns, one should, in principle, be in a position to develop automated or semiautomated programs to speed the assignment process. For proteins, such programs have already been developed for obtaining assignments from homonuclear 3D spectra (Oschkinat et al., 1991).

Cross-talk cross-peaks (Vuister et al., 1990) that we alluded to earlier in our discussion impede the assignment process to a great extent. While a comparison of spectral patterns and cross-peak intensities in adjacent planes can identify these peaks, increased digital resolution in the dimension of analysis can alleviate this problem somewhat. In this respect, the analysis of planes along the acquisition domain (ω_3) is advantageous since the digital resolution along this dimension is not constrained by experimental time.

Structural Implications for the DNA Triplex. The NOE patterns seen in both 2D and 3D spectra for all three strands of the pyrimidine·purine·pyrimidine triplex in Chart I reveal a right-handed helical structure with no disruptions in sequential connectivities despite the introduction of a purine residue (G18) at the center of an otherwise homopyrimidine third strand (Chart I). These conclusions are based on several lines of evidence. No discontinuities are observed while tracing the base–H2′,2″ as well as the base-H1′ sequential connectivities for all three strands in the H1′ and H2′,2″ ω_3 planes of the 3D spectrum. Each of the purine–pyrimidine steps in the stem region of the triplex, including A4–T5, A10–T11, and G18–T19, exhibit base H8–CH_3 NOEs characteristic of right-handed helical structures. A few cross-strand NOEs typical of right-handed duplexes, involving adenine H2 and the H1′ protons of purine and Watson–Crick pyrimidine strands, are also observed. The H2 proton of residue A12, which is the most well-resolved among all H2 protons in the triplex, besides showing an NOE to its own H1′ proton shows NOEs to the H2 and H1′ protons of A4 as well as to the H1′ proton of G13. NOEs involving the remaining H2 protons are undetermined due to overlaps except for the weak intraresidue NOE seen between the A4 H2 and the H1′ protons.

At this stage, the conformation adopted by the two loops connecting the three strands of the triplex is not clear because of the absence of interresidue contacts in these regions. However, in agreement with our data in H_2O, there is evidence for a stacked-in conformation for the first thymidine residue of the loop linking the purine and the pyrimidine strands of the triplex (Chart I). (1) Base–H2′,2″ sequential connectivities can be traced up to the first loop residue (designated TL1) flanking the guanosine G14 on the 3′ side; also, an NOE is observed between the G14 H8 and TL1 methyl protons. (2) The stacking interaction is also reflected in the chemical shift of the H6 proton of TL1 (Table I), which resonates at the most upfield position of all thymidine H6 protons in the loops.

Chart II

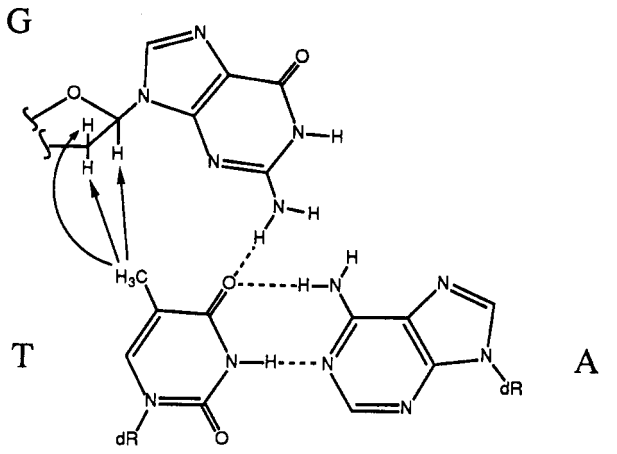

a

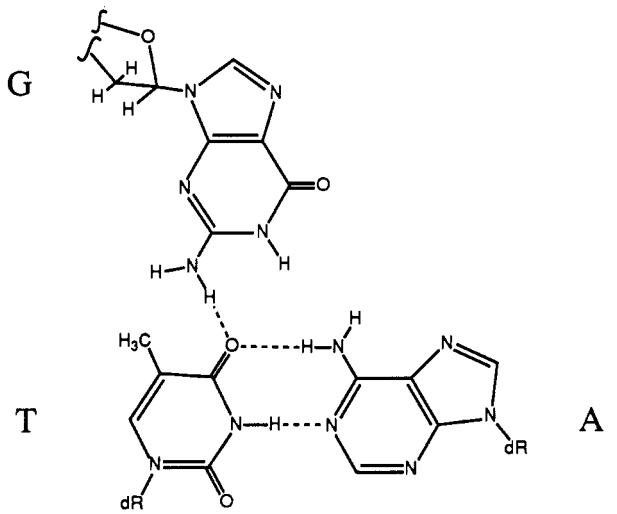

b

Although we were able to assign the base and sugar protons for each of the 10 thymidine residues in the loop regions, the absence of interresidue contacts that we noted earlier prohibited sequence-specific assignments for these residues barring residue TL1 (see above).

The G·TA Triple Site. The amino protons of guanosine have been implicated in hydrogen bonding in the G·TA triple (Griffin & Dervan, 1988). Two base-pairing schemes differing in the amino proton used for this hydrogen-bond formation can be drawn (Chart IIa,b). Our earlier NMR studies in H_2O could not unambiguously identify these protons and as a result could not rule out either of these alternatives (Radhakrishnan et al., 1991a). However, the strong cross-strand NOEs seen between the G18 H1′ proton and the T11 CH_3 protons within the same triple (Table II, Chart IIa) favors the alignment shown in Chart IIa over that in Chart IIb. This has important structural implications since these two base-pairing alignments give rise to significantly different conformations at this site.

Interestingly, a strong intraresidue NOE is observed between the H8 and H3′ protons of guanosine G18. The presence of this cross-peak in the 50-ms 2D NOESY spectrum together with the H1′–H2″ cross-peak pattern in the COSY spectra (data not shown) suggests a predominant N-type sugar conformation for this residue. Moreover, the H3′ and H5′/H5″ protons of G18 exhibit NOEs to the H2″ of T17 (Table II, Figure 7). Whether these unusual interresidue sugar contacts are due to different sugar puckers adopted by contiguous residues in general or whether they are unique to the G·TA triple will be examined by modeling studies.

Strong upfield shifts are observed for T17 H2′,2″ and T19 CH_3 protons, while the T17 H6 proton resonantes at the most upfield position among H6 protons (Table I). Since both residues flank guanosine G18, these effects may result from base-stacking interactions with the G18 purine ring. While the H6 and methyl protons affected by this interaction reflect the right-handed sense of this strand, the behavior of the H2′,2″ protons of T17 suggests that these protons are positioned above the guanine ring. The H1′ and H3′ protons of G18 exhibit contrasting behavior in their chemical shifts. The former is shifted upfield relative to the other H1′ protons while the latter resonates at the most downfield position among H3′ protons. These unusual chemical shifts may augment the existing data on the local conformation.

Interstrand Contacts between the Purine Strand and the Protonated Pyrimidine Strand. Intramolecular triplex formation results in a parallel alignment of the protonated pyrimidine third strand relative to the purine strand (Chart I). Our earlier characterization of the G·TA triplex in H_2O identified NOEs involving imino protons of the third strand and the H8 protons of the purine strand within the same triple which serve as useful markers for monitoring Hoogsteen base-pair formation in a triplex (Radhakrishnan et al., 1991a). Several other NOEs were also detected which involved the imino protons of the third strand and the sugar H2′,2″ protons of the purine strand. From an assignment of these cross-peaks (Table II), it is clear that each thymidine imino proton in the protonated pyrimidine strand is closer to the H2′,2″ protons of the adjacent purine in the 5′ direction than to the H2′,2″ protons of the paired adenosine within the T·AT triple, as schematically depicted in Figure 8.

In contrast to the number of cross-strand connectivities seen in H_2O, only a few NOEs are observed in spectra on the G·TA triplex recorded in D_2O (Table II). Besides, these NOEs are weak and involve the base protons of the purine strand and the H1′ protons of the protonated pyrimidine strand. Specifically, the H1′ proton of a given residue in the third strand shows NOEs to the base proton of the residue preceding its Hoogsteen base-pairing partner, not unlike the trend observed in H_2O (Figure 8B).

Although it is premature to derive detailed structural information about the pyrimidine·purine·pyrimidine triplex containing a central G·TA triple, from the foregoing discussion, a few qualitative features are evident: (1) The bases in the third strand penetrate deeply into the major groove of the Watson–Crick duplex with a bias toward the purine strand, while the sugar moieties interact with their counterparts in the purine strand. These interstrand contacts, as we have shown, can be monitored by NMR using the conventional minor groove proton markers (NH3, H1′, and H2″) in the third strand and the major groove proton markers (H8, thymine methyl, and H2′) in the purine strand. (2) The guanosine G18 adopts a predominantly N-type sugar conformation and preferentially uses one of its amino protons in the recognition of thymine T11 in the G·TA triple. (3) The same guanosine G18 is accommodated within the helix of an otherwise homopyrimidine strand, and structural distortions, if any, seem to be minimal around this site.

A detailed three-dimensional structural model for the G·TA triplex should provide further insights into the conformational aspects of the pyrimidine·purine·pyrimidine triplexes in general, and the G·TA triple in particular. The NOE analysis presented in this paper will be complemented by spectral simulation

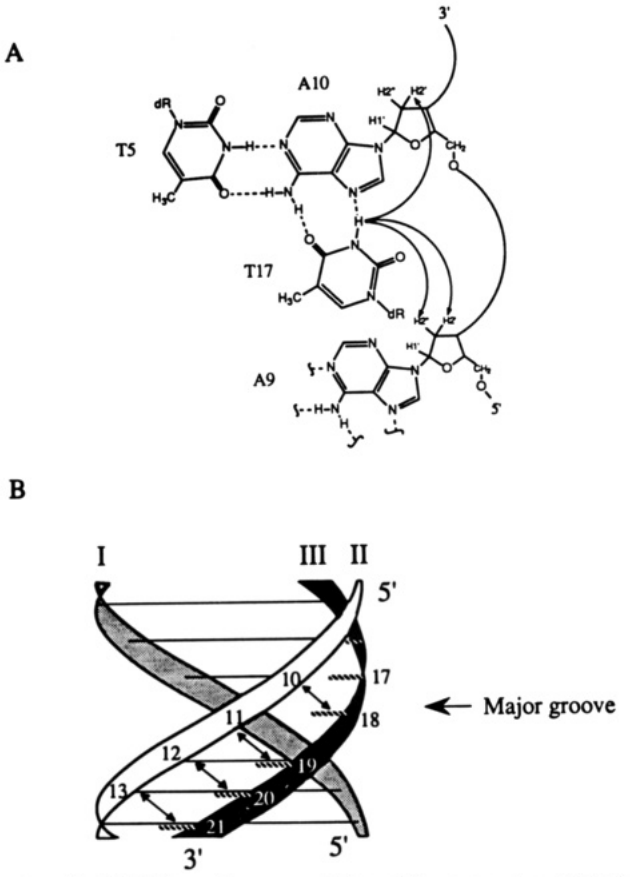

FIGURE 8: (A) Schematic representation of the cross-strand NOEs (shown by arrows) detected in H_2O between the imino proton of T17 and the sugar protons of purine residues A9 and A10 in the G·TA triplex. The other thymidine imino protons in the third strand also exhibit similar patterns. See text for details. (B) Schematic illustration of the interstrand contacts involving residues belonging to adjacent triples in the G·TA triplex. The arrows denote weak NOEs observed between the H1′ protons of the third strand and the base protons of the purine strand and, in addition, moderate NOEs between the imino protons of the third strand and the H2′,2″ protons of the purine strand.

of COSY data sets to arrive at the complete three-dimensional structure of the triplex.

Correction. In our earlier paper (Radhakrishnan et al., 1991a), we had misassigned a cross-peak (peak W, Figure 3B) to the interaction between T17 imino and A10 amino proton pairs. We now attribute this cross-peak to the dipolar interaction between A9 H8 and T17 imino protons. Structurally, this has an important implication since this interaction is consistent with our current data on the relative orientation of the bases and sugars in the purine and Hoogsteen pyrimidine strands. We believe that the other imino protons also show a similar trend, but the evidence is not compelling as the relevant cross-peaks are partially or fully obscured by overlaps.

ACKNOWLEDGMENTS

The NMR spectrometers were purchased from funds donated by the Roberts Woods Johnson Trust toward setting up an NMR Center in the Basic Medical Sciences at Columbia University. The computing support extended by Glaxo Research Institute is gratefully acknowledged by I.R.

REFERENCES

Arnott, S., & Selsing, E. (1974) *J. Mol. Biol. 88*, 509–521.
Arnott, S., Bond, P. J., Selsing, E., & Smith, P. J. C. (1976) *Nucleic Acids Res. 3*, 2459–2470.
Beal, P. A., & Dervan, P. B. (1991) *Science 251*, 1360–1363.
Boelens, R., Vuister, G. W., Koning, T. M. G., & Kaptein, R. (1989) *J. Am. Chem. Soc. 111*, 8525–8526.
Breg, J. N., Boelens, R., Vuister, G. W., & Kaptein, R. (1990) *J. Magn. Reson. 87*, 646–651.
Broitman, S. L., Im, D. D., & Fresco, J. R. (1987) *Proc. Natl. Acad. Sci. U.S.A. 84*, 5120–5124.
Chen, F.-M. (1991) *Biochemistry 30*, 4472–4479.
Cooney, M., Czernuszewicz, G., Postel, E. H., Flint, S. J., & Hogan, M. E. (1988) *Science 241*, 456–459.
de los Santos, C., Rosen, M., & Patel, D. J. (1989) *Biochemistry 28*, 7282–7289.
Fesik, S. W., & Zuiderweg, E. R. P. (1988) *J. Magn. Reson. 78*, 588–593.
Gao, X., & Burkhart, W. (1991) *Biochemistry 30*, 7730–7739.
Greisinger, C., Sorenson, O. W., & Ernst, R. R. (1987a) *J. Magn. Reson. 73*, 574–579.
Greisinger, C., Sorenson, O. W., & Ernst, R. R. (1987b) *J. Am. Chem. Soc. 109*, 7227–7228.
Greisinger, C., Sorenson, O. W., & Ernst, R. R. (1989) *J. Magn. Reson. 84*, 14–63.
Griffin, L. C., & Dervan, P. B. (1989) *Science 245*, 967–971.
Horne, D., & Dervan, P. B. (1990) *J. Am. Chem. Soc. 112*, 2435–2437.
Kohwi, Y., & Kohwi-Shigematsu, T. (1988) *Proc. Natl. Acad. Sci. U.S.A. 85*, 3781–3785.
Letai, A. G., Pallindino, M. A., Fromin, E., Rizzo, V., & Fresco, J. R. (1988) *Biochemistry 27*, 9108–9112.
Luebke, K. J., & Dervan, P. B. (1989) *J. Am. Chem. Soc. 111*, 8733–8735.
Maher, L. J., III, Wold, B., & Dervan, P. B. (1989) *Science 245*, 725–730.
Manzini, G., Xodo, L. E., Gasparotto, D., & Quadrifoglio, F. (1990) *J. Mol. Biol. 213*, 833–843.
Marion, D., Kay, L. E., Sparks, S. W., Torchia, D. A., & Bax, A. (1989) *J. Am. Chem. Soc. 111*, 1515–1517.
Mooren, M. M., Pulleyblank, D. E., Wijmenga, S. S., Bloomers, M. J., & Hilbers, C. W. (1990) *Nucleic Acids Res. 18*, 6523–6529.
Mooren, M. M. W., Hilbers, C. W., van der Marel, G. A., van Boom, J. H., & Wijmenga, S. S. (1991) *J. Magn. Reson. 94*, 101–111.
Moser, H. E., & Dervan, P. B. (1987) *Science 238*, 645–650.
Oschkinat, H., Greisinger, C., Kraulis, P. J., Sorenson, O. W., Ernst, R. R., Gronenborn, A., & Clore, G. M. (1988) *Nature 332*, 374–376.
Oschkinat, H., Cieslar, C., Holak, T. A., Clore, G. M., & Gronenborn, A. M. (1989a) *J. Magn. Reson. 83*, 450–472.
Oschkinat, H., Cieslar, C., Gronenborn, A. M., & Clore, G. M. (1989b) *J. Magn. Reson. 81*, 212–216.
Oschkinat, H., Holak, T. A., & Cieslar, C. (1991) *Biopolymers 31*, 699–712.
Padilla, A., Vuister, G. W., Boelens, R., Kleywegt, G. J., Cave, A., Parello, J., & Kaptein, R. (1990) *J. Am. Chem. Soc. 112*, 5024–5030.
Perronault, L., Asseline, U., Rivalle, C., Thuong, N. T., Bisagni, E., Giovannangeli, C., Le Deon, T., & Helene, C. (1990) *Nature 344*, 358–360.
Pilch, D. S., Levenson, C., & Shafer, R. H. (1990) *Proc. Natl. Acad. Sci. U.S.A. 87*, 1942–1946.
Pilch, D. S., Levenson, C., & Shafer, R. H. (1991) *Biochemistry 30*, 6081–6087.
Piotto, M. E., & Gorenstein, D. G. (1991) *J. Am. Chem. Soc. 113*, 1438–1440.
Plum, G. E., Park, Y. W., Singleton, S. F., Dervan, P. B., & Breslauer, K. J. (1990) *Proc. Natl. Acad. Sci. U.S.A. 87*, 9436–9440.

Povsic, T. J., & Dervan, P. B. (1989) *J. Am. Chem. Soc. 111*, 8733–8735.
Praseuth, D., Perronault, L., Le Doan, T., Chassignol, M., Thuong, N., & Helene, C. (1988) *Proc. Natl. Acad. Sci. U.S.A. 85*, 1349–1353.
Radhakrishnan, I., Gao, X., de los Santos, C., Live, D., & Patel, D. J. (1991a) *Biochemistry 30*, 9022–9030.
Radhakrishnan, I., de los Santos, C., & Patel, D. J., (1991b) *J. Mol. Biol. 221*, 1403–1418.
Radhakrishnan, I., Patel, D. J., & Gao, X. (1991c) *J. Am. Chem. Soc. 113*, 8542–8544.
Rajagopal, P., & Feigon, J. (1989) *Biochemistry 28*, 7859–7870.
Sklenar, V., & Feigon, J. (1990) *Nature 345*, 6836–6838.
Strobel, S. A., & Dervan, P. B. (1990) *Science 249*, 73–75.
Strobel, S. A., & Dervan, P. B. (1991) *Nature 350*, 172–174.
Sun, J. S., Francois, J. C., Montenay-Gartesier, T., Saison-Behmoras, T., Roig, V., Thuong, N. T., & Helene, C. (1989) *Proc. Natl. Acad. Sci. U.S.A. 86*, 9198–9202.
Vuister, G. W., Boelens, R., & Kaptein, R. (1988) *J. Magn. Reson. 80*, 176–185.
Vuister, G. W., Boelens, R., Padilla, A., Kleywegt, G. J., & Kaptein, R. (1990) *Biochemistry 29*, 1829–1839.
Wells, R. D., Collier, D. A., Hanvey, J. C., Shimizu, M., & Wohlraub, F. (1988) *FASEB J. 2*, 2939–2949 (and references cited therein).
Wüthrich, K. (1986) *NMR of Proteins and Nucleic Acids*, Wiley, New York.
Xodo, L. E., Manzini, G., & Quadrifoglio, F. (1990) *Nucleic Acids Res. 18*, 3557–3564.
Zuiderweg, R. P., & Fesik, S. W. (1989) *Biochemistry 28*, 2387–2391.

Chromophore Configuration of *pharaonis* Phoborhodopsin and Its Isomerization on Photon Absorption†

Yasushi Imamoto,‡ Yoshinori Shichida,*,‡ Junichi Hirayama,§ Hiroaki Tomioka,§,∥ Naoki Kamo,§ and Tôru Yoshizawa⊥

Department of Biophysics, Faculty of Science, Kyoto University, Kyoto 606-01, Japan, Department of Biophysical Chemistry, Faculty of Pharmaceutical Sciences, Hokkaido University, Sapporo 060, Japan, and Department of Applied Physics and Chemistry, The University of Electro-Communications, Chofu, Tokyo 182, Japan

Received September 18, 1991; Revised Manuscript Received December 16, 1991

ABSTRACT: The configuration of the retinylidene chromophore in *pharaonis* phoborhodopsin (ppR) and its changes during the photoreaction cycle were investigated by means of a chromophore extraction method followed by HPLC analysis. The ppR has an all-trans chromophore, and unlike bacteriorhodopsin, it exhibits no dark isomerization of the chromophore. Irradiation of a ppR sample in the presence of 10 mM hydroxylamine, at which concentration a negligible amount of ppR was bleached, caused the formation of 90% 13-*cis*- and 10% *all-trans*-retinal oximes. Because the ppR sample under the continuous irradiation was a mixture containing original ppR, ppR_M, and a small amount of ppR_O, the above results showed that the chromophores of ppR_M and ppR_O are in a 13-cis form and an all-trans form, respectively. Therefore, the all-trans chromophore of ppR is isomerized to the 13-cis form on photon absorption, and it is thermally reisomerized to the all-trans form on the conversion process from ppR_M to ppR_O. The extracted retinal oximes from ppR and ppR_O were mainly the 15-syn form, while that from ppR_M was mainly the 15-anti form. This fact indicated that the attack of hydroxylamine on the chromophore is stereoselective owing to the unique structure of the chromophore binding site near the Schiff base region of the chromophore.

Negative phototactic response of a haloalkaliphilic bacterium, *Natronobacterium pharaonis*, is mediated by a retinal protein called *pharaonis* phoborhodopsin (ppR)[1] (Tomioka et al., 1990). It is very similar in its physiological functions (Takahashi et al., 1985; Tomioka et al., 1986) and spectroscopic properties (Bivin & Stoeckenius, 1986; Imamoto et al., 1991; Hirayama et al., 1992) to phoborhodopsin (pR) of *Halobacterium halobium*. The ppR has an absorption maximum at 498 nm, which is a 10 nm longer wavelength than that of pR, while both of the absorption spectra exhibit vibrational fine structures even at room temperature (Tomioka et al., 1990; Takahashi et al., 1990). Furthermore, our previous investigations of pR and ppR by low-temperature spectrophotometry revealed that they show very similar photochemical and subsequent thermal reactions to each other

† This work was supported in part by a Grant-in-Aid for Scientific research from the Japanese Ministry of Education, Culture and Science, by a Special Coordination Fund of the Science and Technology Agency of Japanese government, by a Grant from the Human Frontier Science Program, and by a Ciba-Geigy Foundation (Japan) for the Promotion of Science.

* Correspondence should be addressed to this author.
‡ Kyoto University.
§ Hokkaido University.
∥ Present address: Laboratory for Bioelectronic Materials, Frontier Research Program, Riken Institute, Wako 351-01, Japan.
⊥ The University of Electro-Communications.

[1] Abbreviations: ppR, *pharaonis* phoborhodopsin; pR, phoborhodopsin; bR, bacteriorhodopsin; hR, halorhodopsin; sR, sensory rhodopsin; HPLC, high-performance liquid chromatography; Ts, *all-trans*-15-*syn*-retinal oxime; Ta, *all-trans*-15-*anti*-retinal oxime; 13s, 13-*cis*-15-*syn*-retinal oxime; 13a, 13-*cis*-15-*anti*-retinal oxime.

0006-2960/92/0431-2523$03.00/0